

Nanoscale stratification of optical excitation in self-interacting one-dimensional arrays

A. E. Kaplan* and S. N. Volkov

Department of Electrical and Computer Engineering, Johns Hopkins University, Baltimore, Maryland 21218, USA

(Received 26 January 2009; published 18 May 2009)

The major assumption of the Lorentz-Lorenz theory about uniformity of local fields and atomic polarization in dense material does not hold in finite groups of atoms, as we reported earlier [A. E. Kaplan and S. N. Volkov, Phys. Rev. Lett. **101**, 133902 (2008)]. The uniformity is broken at subwavelength scale, where the system may exhibit strong stratification of local field and dipole polarization, with the strata period being much shorter than the incident wavelength. In this paper, we further develop and advance that theory for the most fundamental case of one-dimensional arrays, and study nanoscale excitation of so-called “locsitons” (local field excitations) and their standing waves (strata) that result in size-related resonances and related large field enhancement in finite arrays of atoms. The locsitons may have a whole spectrum of spatial frequencies, ranging from long waves, to an extent reminiscent of ferromagnetic domains, to supershort waves, with neighboring atoms alternating their polarizations, which are reminiscent of antiferromagnetic spin patterns. Of great interest is the different kind of “hybrid” mode of excitation, greatly departing from any magnetic analogies. We also study differences between Ising-type near-neighbor approximation and the case where each atom interacts with all other atoms in the array. We find an infinite number of “exponential eigenmodes” in the lossless system in the latter case. At certain “magic” numbers of atoms in the array, the system may exhibit self-induced (but linear in the field) cancellation of resonant local-field suppression. We also studied nonlinear modes of locsitons and found optical bistability and hysteresis in an infinite array for the simplest modes.

DOI: [10.1103/PhysRevA.79.053834](https://doi.org/10.1103/PhysRevA.79.053834)

PACS number(s): 42.65.Pc, 85.50.-n

I. INTRODUCTION

This paper is a theoretical extension of our recent letter [1] on nanoscale stratification of local field (LF) and atomic dipole excitation in low-dimensional lattices driven by a laser at the frequency of the resonant atomic transition. We focus here on the most fundamental case of a one-dimensional (1D) array of resonant atoms, and construct a detailed theory of both linear and nonlinear interactions in the system, resulting in such phenomena as subwavelength spatial modulation (stratification) of polarization and local field, long-wave (LW) and short-wave (SW) stratifications, size-related resonances and large field enhancement, “magic” numbers, ferromagnetic- and antiferromagneticlike atomic polarizations, optical bistability and hystereses. In addition to the results [1] and their derivations, we also present here results (i) on the size-related resonances using a many-body approximation involving interactions of each atom with all other atoms in the array, beyond the Ising-type approximation whereby atoms only interact with their nearest neighbors; (ii) on traveling local field excitation (“locsiton”) waves and their dissipation, as well as an estimate of the maximum size of the 1D array to support most of the effects discussed here; (iii) on hystereses and optical bistability in arbitrarily long arrays; and (iv) on general mathematical consideration of dispersion relation in the self-interacting arrays for dipole approximation and beyond it.

It is well known that optical properties of sufficiently dense materials are substantially affected by the near-field interactions between neighboring particles at the frequency of the incident field, in particular, quasistatic (nonradiative)

dipole interactions. The best-known manifestation of this fact is the *local vs incident field* phenomenon and related Lorentz-Lorenz or Clausius-Mossotti relations [2] for dielectric constant as a nonlinear function of the number density. The microscopic field (or LF) \mathbf{E}_L acting upon atoms or molecules becomes then different from both the applied and average macroscopic fields because of interparticle interaction. In the most basic case, that relation between \mathbf{E}_L and the average field \mathbf{E} is $\mathbf{E}_L = (\epsilon + 2)\mathbf{E}/3$, where ϵ is the dielectric constant of the material at the laser frequency ω . It is worth noting that we are not interested here in the relation between ϵ and the number density of the material, since in the case of small 1D or two-dimensional (2D) arrays the issue is moot. For the same reason, it also makes sense to deal directly with the incident field \mathbf{E}_{in} instead of the averaged field. In most theories of those interactions a traditional standard (and at that often implicit) assumption, reflected also in the above formula, is that the local field and polarization are uniform in the near neighborhood of each particle at least at the distances shorter than the wavelength of light, λ . This essentially amounts to the so-called mean-field approximation.

It was shown by us [1], however, that if the *local uniformity* is not presumed, then, under certain conditions on the particle density and their dipole strengths, the system of interacting particles is bound to exhibit periodic spatial variations of polarization and local-field amplitude. These variations result in subwavelength strata with a nanoscale period much shorter than λ . Under certain conditions, the system may exhibit an ultimate nonuniformity, whereby each pair of neighboring atoms in 1D arrays has their dipoles counteroscillating with respect to each other; i.e., their excitations and thus local fields have opposite signs.

To a certain extent this is reminiscent of the situation in magnetic materials with *ferromagnetic vs antiferromagnetic* effects. Indeed, the mean-field approximation, which is at the

*alexander.kaplan@jhu.edu

root of the Curie-Weiss theory of *ferromagnetism* [3], is based on the assumption of uniform polarization of all the neighboring magnetic dipoles even without external magnetic field, when taking into account their interaction with each other. Contrary to that, the Ising theory [3], which does not make the assumption of uniformity, showed that even in the near-neighbor approximation (NNA) for that interaction, the excitation may result in counterpolarization of neighboring atoms in 1D arrays, and thus in a new phenomenon of *antiferromagnetism*. Note here that in these effects there is no notion of “local” vs “external” field phenomenon: in a “pure” case of either of the magnetic effects, no external field is applied. The effects here are the result of self-organization of permanent, “hard,” atomic dipoles with pre-existing dc dipole fields, without any “help from outside.”

In this lies a profound difference between dc magnetic material phenomena (ferro- and antiferromagnetism) on one hand and the effects considered by us here and in [1] on the other hand, all of which are based on the *optical* (or, in general, any other quantum or classical resonance) excitation of atoms (or other small particles, e.g., quantum dots, clusters, and small-particle plasmons). While magnetic dipoles in ferromagnetics are nonzero even in the absence of an external field (we may call them hard dipoles), the oscillating dipoles (in the linear case) can be induced only by the driving field at the near-resonant frequency, so they can be called “soft” dipoles; without such a driving their polarization vanishes. Because in dense material the atoms actually are acted upon by *local* field, the response of each one of them may differ from the others by phase and amplitude (or even direction), with some of the dipoles fully suppressed, while others fully excited. Thus the effects considered here are induced by the interplay of external and local fields, which puts the entire phenomenon squarely into the domain of relations between the local and incident fields. Because of that, since the phenomenon depends strongly on the characteristics of the incident field (polarization, frequency, and, in the nonlinear case, intensity), the spatial modulation of the dipole excitation and local field can vary substantially. This results in a wealth of different patterns, some of them reminiscent of the ferromagnetic pattern, others of the antiferromagnetic pattern, but most of them forming all kinds of hybrid patterns. The complete crossover from ferromagneticlike to antiferromagneticlike state of the system with all the intermediate states can be attained then by simply tuning laser frequency.

Another significant difference here is that the system size is small. Provided there is sufficiently strong interparticle interaction, the new phenomenon can occur in the vicinity of boundaries, lattice defects, impurities or in sufficiently small group of atoms. Recent advances in technology allow fabrication of nanoscale structures with small numbers of atoms. Thus, our theory emphasizes phenomena in relatively small ordered arrays of interacting atoms, in contrast to, e.g., microscopic models of ferromagnetism that mostly focus on averaged, “thermodynamic” perspective on sufficiently large systems. This brings forward an unusual set of nanoscale phenomena. Harking back to ferromagnetic systems, this new emphasis may reveal similar phenomena for nanoscale magnetic systems, which could be an exciting topic for a separate study.

Our choice of 1D and 2D dielectric systems based on the arrays or lattices of atoms, quantum dots, clusters, molecules, etc., allows to control anisotropy of near-field interaction. It also eliminates the issues of electromagnetic (EM) propagation being modified by the effects as the EM wave propagates through the structure (especially if it propagates normally to the lattice).

If *local uniformity* is broken by any perturbation, the system may exhibit near-periodic spatial sub- λ patterns (strata) of polarization. In general, two major modes of the strata transpire: *SW* strata, with the period of up to four interatomic spacings l_a , and *LW* strata. The strata are standing waves of elementary LF excitations (called *locsitons* in [1]) having a near-field, electrostatic nature and low group velocity.

In the first approximation, the phenomenon is linear in the driving field, and the locsitons may be excited within a spectral band much broader than the atomic linewidth. It can be viewed as a Rabi broadening of an atomic line by interatomic interactions. The strata are controlled by laser polarization and the strength of atom coupling, Q , via atomic density, dipole moments, relaxation, and detuning. Once $|Q| > Q_{cr} = O(1)$, the LF uniformity can be broken by boundaries, impurities, vacancies in the lattice, etc. A striking manifestation of the effect is large field resonances due to locsiton eigenmodes in finite lattices, and—at certain magic numbers of atoms in the lattice—almost complete cancellation of field suppression at the atomic resonance. Saturation nonlinearity results in hystereses and optical bistability.

The paper is structured as follows. In Sec. II we derive the main equations for self-interacting atomic lattices of arbitrary dimensions using two-level (nonlinear in general) model for atomic resonances and dipole-dipole interaction between atoms, while Sec. III is on specific equations for linear infinite and finite 1D arrays. In Sec. IV we develop the general theory of locsitons and derive the dispersion relation. In Sec. V we study locsiton band formation, size-related resonances due to standing waves of locsitons (strata), and local-field enhancement. In Sec. VI we concentrate on detailed theory of resonances beyond the near-neighbor approximation, including evanescent solutions (see also Sec. IV). Magic numbers are considered in Sec. VII. In Sec. VIII, we study the effects of losses on locsiton excitation, depth of penetration, and traveling locsiton waves. Sec. IX is on nonlinear locsiton modes, in particular, optical bistability and hysteresis. Section X addresses potential applications of locsitons and their analogies in other physical systems. In Conclusions, Sec. XI, we summarize our results. The Appendix is on general mathematical aspects of dispersion relations for 1D arrays.

II. MAIN EQUATIONS

Our model is based on the near-field dipole atomic interactions, with the incident frequency ω being nearly resonant to an atomic transition with a dipole moment \mathbf{d}_a at the frequency ω_0 . In the linear case, i.e., when the laser intensity is significantly lower than that for the quantum transition saturation (see below), the result of this model coincides with that of a classical harmonic oscillator formed by an electron

in a harmonic potential with the same resonant frequency ω_0 and with the dipole moment

$$|d_a| = \frac{e}{2\pi} \sqrt{\frac{\lambda_C \lambda}{2}}, \quad (2.1)$$

where $\lambda_C = 2\pi\hbar/mc$ is the Compton wavelength of electron.

In a standard LF situation, $\lambda \gg l_a$, where $\lambda = 2\pi c/\omega$, the field of an elementary dipole with the polarization \mathbf{p} is dominated in its near vicinity by a nonradiative, quasistatic (and only electric) component, which is strongly anisotropic in space. This dominant term in the near-field area, $|\mathbf{r}' - \mathbf{r}| = r_0 \ll \lambda$, attenuates as $1/r_0^3$ (see, e.g., [4], Sec. 72). At $|d_a| \ll r_0 \ll \lambda$ the amplitude of the field of an oscillating dipole located at \mathbf{r}' induces a field at the point of observation \mathbf{r} with the amplitude coinciding with that of an elementary static dipole with the same polarization \mathbf{p}' :

$$\mathbf{E}_{\text{dp}}(\mathbf{r}', \mathbf{r}) = \frac{3\mathbf{u}(\mathbf{p}' \cdot \mathbf{u}) - \mathbf{p}'}{\epsilon |\mathbf{r}' - \mathbf{r}|^3}, \quad (2.2)$$

where $\mathbf{u} = (\mathbf{r} - \mathbf{r}')/r_0$ is a unit vector in the direction of observation, and ϵ is a background dielectric constant.

We will model a resonant atomic transition by a basic two-level atom in a steady-state mode under the action of a field, $\mathbf{E} \exp(-i\omega t)/2 + \text{c.c.}$, with the amplitude \mathbf{E} and frequency ω , and assume that $l_a \gg |d_a|/e$, so that the wave functions of neighboring atoms do not overlap. Using a semiclassical approach standard in LF theory of resonant atoms [5,6], we can now find the atomic polarization as

$$\mathbf{p} = - \frac{2|d_a|^2 \mathbf{E} \Delta N}{\hbar \Gamma \delta + i}, \quad (2.3)$$

where \mathbf{p} is the polarization amplitude [the full polarization is then $\mathbf{p} \exp(-i\omega t)/2 + \text{c.c.}$]; $\Delta N = N_1 - N_2$ is the population difference, with N_1 and N_2 being atomic populations at respective ground and excited levels ($N_1 + N_2 = 1$); $\delta = T\Delta\omega = T(\omega - \omega_0)$ is a dimensionless detuning from the resonant frequency ω_0 of the two-level atom; $T = 2/\Gamma$ is a *transverse* relaxation time (the time of polarization relaxation); and Γ is the (homogeneous) linewidth of the linear resonance [7]. In turn, the steady-state population difference is [5]

$$\Delta N = N^{\text{eq}} \left(1 + T\tau \frac{|d_a E/\hbar|^2}{1 + \delta^2} \right)^{-1}, \quad (2.4)$$

where τ is a *longitudinal* relaxation time (lifetime of the excited atom), and N^{eq} is an equilibrium population difference at the system temperature due to Boltzmann's distribution. In optics one can usually assume $N^{\text{eq}} \approx 1$, so that

$$\Delta N \approx \left[1 + \frac{|E|^2/E_{\text{sat}}^2}{1 + \delta^2} \right]^{-1} \equiv f_{\text{NL}}(|E|^2), \quad (2.5)$$

$$E_{\text{sat}}^2 = \frac{\hbar^2}{|d_a|^2 \tau T},$$

where E_{sat}^2 is the saturation intensity, and $f_{\text{NL}}(|E|^2)$ is nonlinearity due to saturation. Substituting Eq. (2.5) into Eq. (2.3), one obtains a closed-form expression for the polarization,

$$\mathbf{p} = - \mathbf{E} \frac{2|d_a|^2}{\hbar \Gamma (\delta + i)} f_{\text{NL}}(|E|^2). \quad (2.6)$$

For a classical harmonic (linear) oscillator we have

$$\mathbf{p} = - \frac{\mathbf{E} e^2}{\omega_0 \Gamma m (\delta + i)}, \quad (2.7)$$

where m is the mass of electron.

The local field $\mathbf{E}_L(\mathbf{r})$ at each atom is the incident laser field \mathbf{E}_{in} plus the sum of the near fields $\mathbf{E}_{\text{dp}}(\mathbf{r}', \mathbf{r})$ [Eq. (2.2)] induced by all the surrounding dipoles at \mathbf{r}' acted upon by the respective local fields $\mathbf{E}_L(\mathbf{r}')$; i.e.,

$$\mathbf{E}_L(\mathbf{r}) = \mathbf{E}_{\text{in}}(\mathbf{r}) + \sum_{\text{latt}}^{\mathbf{r}' \neq \mathbf{r}} \mathbf{E}_{\text{dp}}(\mathbf{r}', \mathbf{r}) = \mathbf{E}_{\text{in}}(\mathbf{r}) + \frac{1}{\epsilon} \sum_{\text{latt}}^{\mathbf{r}' \neq \mathbf{r}} \frac{3\mathbf{u}(\mathbf{p}' \cdot \mathbf{u}) - \mathbf{p}'}{|\mathbf{r}' - \mathbf{r}|^3}, \quad (2.8)$$

where \sum_{latt} denotes summation over the entire lattice or array. To obtain a closed-form master equation, e.g., for $\mathbf{E}_L(\mathbf{r})$ alone, we use Eq. (2.6) to write

$$\mathbf{E}_L(\mathbf{r}) = \mathbf{E}_{\text{in}}(\mathbf{r}) - \frac{Q}{4} \sum_{\text{latt}}^{\mathbf{r}' \neq \mathbf{r}} \left| \frac{l_a}{|\mathbf{r}' - \mathbf{r}|} \right|^3 \times \{3\mathbf{u}[\mathbf{E}_L(\mathbf{r}') \cdot \mathbf{u}] - \mathbf{E}_L(\mathbf{r}')\} f_{\text{NL}}[|\mathbf{E}_L(\mathbf{r}')|^2], \quad (2.9)$$

where $\mathbf{E}_L(\mathbf{r})$ are local fields only at the locations of atoms in the lattice and not at any other points inside or outside it. $Q = Q_a/(\delta + i)$ is a tuning-dependent strength of dipole-dipole interaction, and the maximum absolute strength Q_a is

$$Q_a = \frac{8|d_a|^2}{\epsilon \hbar \Gamma l_a^3} = \frac{4\alpha \lambda_0 (|d_a|/e)^2 \omega_0}{\pi \epsilon l_a^3 \Gamma}, \quad (2.10)$$

where $\alpha = e^2/\hbar c \approx 1/137$ is the fine-structure constant, and nonlinear factor f_{NL} is as in Eq. (2.5). For a classical harmonic oscillator [Eq. (2.1)], we have

$$(Q_a)_{\text{class}} = \frac{4e^2}{\epsilon m \omega_0 \Gamma l_a^3} = \frac{1}{\epsilon \pi^2} \frac{r_e \lambda_0^2 \omega_0}{l_a^3 \Gamma}, \quad (2.11)$$

where $r_e \equiv e^2/m_e c^2 \approx 2.8 \times 10^{-6}$ nm is the classical radius of electron.

Equations (2.8) and (2.9) reflect many-body nature of the interaction. A conventional approach to local fields within the Lorentz-Lorenz theory is to look for a self-consistent solution for the fields in this interaction, with an assumption, however, that they are *uniform* (the mean-field theory), i.e., to set $\mathbf{E}_L(\mathbf{r}) = \mathbf{E}_L(\mathbf{r}')$ and also use an encapsulating sphere around the observation point. These assumptions effectively shut out any strong spatial variations in the atomic excitations and local field that may exist at the interatomic scale. That is where we depart from the Lorentz-Lorenz theory; *none of those assumptions is used here*, and our approach is to use general expression (2.8) or (2.9) and seek straightforward solution for them.

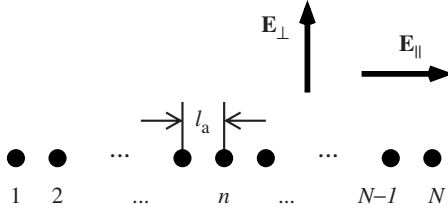


FIG. 1. 1D array of atoms and laser light with different polarizations; light is incident normally to the plane of the graph.

We will see below that the major critical condition for the phenomenon to exist and be observable at least at other optimal conditions is that Q_a exceeds some critical value, $Q_a > O(1)$. Three parameters are critical in this respect: atomic dipole moment d_a , the spacing l_a between atoms, and the atomic linewidth Γ , since $Q_a \propto |d_a|^2 / \Gamma l_a^3$. To get an idea of whether the above critical condition is realistic, let us look first at the case of a gaslike collection of atoms, with the relaxed requirement on the spacing l_a . Large dipole moments and narrow resonances in, e.g., *alkali* vapors [6] or CO_2 gas [5], solids [8], quantum wells, and clusters may greatly enhance the phenomenon and allow for l_a from subnanometer to a few tens of nanometers. Considering an example with $l_a \sim 100 \text{ \AA}$, corresponding to the volume density of $\sim 10^{18} \text{ cm}^{-3}$, $|d_a|/e \sim 1 \text{ \AA}$, $\lambda_0 \sim 1 \text{ \mu m}$, $\epsilon = 1$, and $\Gamma/\omega_0 \sim 10^{-6}$, all of which are reasonable data, we obtain $Q_a \sim 10^2$, which provides a margin large enough to see all the effects discussed here. It is also of interest to roughly estimate what is the upper limit for Q_a . To that end, consider the extreme situation of $l_a \sim |d_a|/e$ (solid-state-like or liquidlike packing of participating atoms), in which case we have the ceiling for Q_a as

$$Q_{\text{ceil}} = \frac{8e^3}{\epsilon \hbar \Gamma |d_a|} = \frac{4\alpha}{\pi \epsilon} \frac{\lambda_0}{(|d_a|/e)} \frac{\omega_0}{\Gamma}. \quad (2.12)$$

Even taking into consideration significant line broadening Γ , Q_{ceil} may exceed unity by many orders of magnitude, thus providing huge margin for the existence and observation of locsitons and related effects.

III. 1D ARRAY OF ATOMS: LINEAR CASE

We consider here the most basic model of a 1D array of N atoms lined up along the z axis, spaced by l_a , and driven by a laser propagating normally to the array and having an arbitrary polarization (Fig. 1). In the linear case, $|E_L|^2 \ll E_{\text{sat}}^2$, when in Eq. (2.9) $f_{\text{NL}} = 1$, it is sufficient to consider effects caused by linearly polarized light with either one of the two mutually orthogonal polarizations. Any other polarization (e.g., a circular one) can be treated as a linear combination of those two. In the case of a 1D array, natural choices for these two basic configurations are

(a) the incident field \mathbf{E}_{in} is parallel to the z axis, $\mathbf{E}_{\text{in}} \parallel \hat{\mathbf{e}}_z$ (and the dipoles line up “head to tail;” we will call it \parallel configuration); and

(b) \mathbf{E}_{in} is normal to the z axis, $\mathbf{E}_{\text{in}} \perp \hat{\mathbf{e}}_z$ (“side-by-side” lineup; \perp configuration).

The general solution will be a linear vectorial superposition of these two. This choice of the basic configurations is dictated by the simplicity of the resulting polarization of the local field. Indeed, in both cases, it follows that the polarization of local field is parallel to that of the incident field, $\mathbf{E}_L \parallel \mathbf{E}_{\text{in}}$, so we can use scalar equations for all fields. Using the dimensionless notation $\mathcal{E}_n = [E_L(\mathbf{r}_n)/E_{\text{in}}]_{(p)}$, where (p) denotes polarization, $(p) = \parallel$ or $(p) = \perp$, and recalling that now $\mathbf{u} \parallel \hat{\mathbf{e}}_z$, we write Eq. (2.9) for both configurations as

$$\mathcal{E}_n + QF_{(p)} \sum_{1 \leq j \leq N}^{j \neq n} \frac{\mathcal{E}_j/2}{|j-n|^3} = 1 \quad \text{if } n = 1, \dots, N, \\ \mathcal{E}_n = 0 \quad \text{otherwise}, \quad (3.1)$$

where $F_{(p)}$ is a form factor due to polarization configuration: $F_{\parallel} = 1$ and $F_{\perp} = -1/2$.

If the 1D array is infinite, $N \rightarrow \infty$, or sufficiently long, $N \gg 1$, it is instructive to rewrite Eq. (3.1) in the form

$$\mathcal{E}_n + SQF_{(p)} \sum_{-\infty \leq j \leq \infty}^{j \neq n} \frac{\mathcal{E}_j/2S}{|j-n|^3} = 1, \quad (3.2)$$

where $S = \sum_{j=1}^{\infty} j^{-3} \approx 1.202057$. The sums over $|j-n|^{-3}$ in Eqs. (3.1) and (3.2) converge rather fast; hence $S-1$ is not too large (see also the Appendix). Equations (3.1) and (3.2), the same as master equation (2.9), represent the case of *fully interacting arrays* (FIAs), whereby each atom “talks” to all the other atoms in the array, which presents a challenge to an analytical treatment. Of course, a linear Eq. (3.1) for \mathcal{E}_n is solved analytically using a standard linear algebra approach with matrices. However, analyzing the results for large-size arrays, $N \gg 1$, in particular analytically finding all the resonances in $(\mathcal{E}_n)_{\text{max}}(\delta)$, can only be done by using numerical matrix solver, even if we neglect the dissipation.

Thus, there is a need for a simple approximation that would preserve most of the qualitative features of the phenomenon, yet could be easily analyzed analytically. This can be done by using the NNA, similar to that of the Ising model of (anti)ferromagnetism, in which the full sum in Eq. (3.1) and (3.2) is replaced by the sum over the nearest neighbors,

$$\mathcal{E}_n + \frac{QF_{(p)}}{2} (\mathcal{E}_{n-1} + \mathcal{E}_{n+1}) = 1, \\ \mathcal{E}_0 = \mathcal{E}_{N+1} = 0. \quad (3.3)$$

In the ultimate two-atom case, $N=2$ [1], the two approaches merge. The further two-near-neighbors approximation (2-NNA) and even three-near-neighbors approximation (3-NNA) are considered in Sec. VI. We found, however, that in general, a full summation (FIA) in Eq. (3.1), on one hand, and NNA (3.3) as well as 2-NNA, on the other hand, produce qualitatively similar results that differ by a factor of $O(1)$.

Since effects discussed here are most pronounced in relatively small systems or in the small vicinity of perturbations in large lattices, it is natural to stipulate that the *incident* field within the array is uniform, unless stated otherwise. However, this condition can readily be arranged even for an array larger than λ . One of the solutions for the local field (and

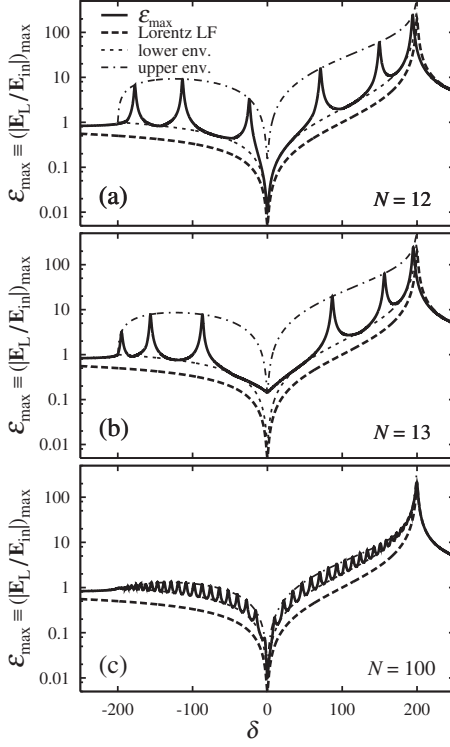


FIG. 2. Spectra of *absolute* maximum local-field amplitudes near an atomic resonance ($\delta=0$) in the near-neighbor approximation with $\delta_{LL}=200$: (a) locsiton resonances with 12 atoms in the array; (b) the same with 13 (magic number) atoms in the array; and (c) merging and damping of locsiton resonances for a large number of atoms, $N=100$. The curves show the amplitudes of local fields for size-related resonances, local fields due to Lorentz-Lorenz theory, and lower and upper amplitude envelopes of the resonances.

atomic excitation) in the *infinite* 1D array (or a sufficiently long one, whereby we can neglect edge effects) is also uniform. We will call it the “Lorentz” solution $\bar{\mathcal{E}}$, to be found from Eq. (3.2) by setting $\mathcal{E}_n = \mathcal{E}_j = \bar{\mathcal{E}}$ as

$$\bar{\mathcal{E}}_{(p)} = \frac{1}{1 + QS F_{(p)}} = \frac{1}{1 - [(\delta_{LL})_{(p)} / (\delta + i)]},$$

$$(\delta_{LL})_{(p)} = -SQ_a F_{(p)}, \quad (3.4)$$

where we introduced polarization-dependent parameter δ_{LL} , which determines Lorentz-Lorenz shift at $\delta = \delta_{LL}$ (see below); $|\delta_{LL}|$ is a measure of the polarization-related strength of interaction. Equation (3.4) may be viewed as a 1D counterpart of the *Lorentz-Lorenz* relation for local field. Notice, however, that the field $\bar{\mathcal{E}}$ is strongly *anisotropic* with respect to the polarization. The spectral behavior of $|\bar{\mathcal{E}}|$ is depicted in Fig. 2 with thicker dashed curves in all the graphs.

If $Q_a \gg 1$, it shows, as one may expect, a deep dip at the atomic resonance frequency, i.e., at $\delta=0$,

$$|\bar{\mathcal{E}}_{(p)}|_{\min}^2 = \frac{1}{1 + \delta_{LL}^2} \quad (3.5)$$

(so that at the atomic resonance the local field is suppressed, as if it is pushed out of the array), and a strong new resonant

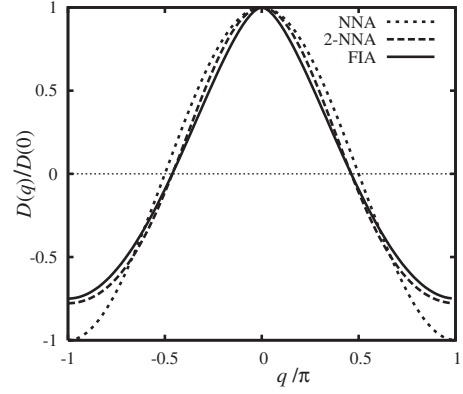


FIG. 3. Dispersion relations for an infinite array and negligible losses, i.e., normalized laser detuning δ/δ_{LL} vs the normalized wave number q/π . Curves show the dispersions for NNA (4.2), 2-NNA (6.6), and FIA, whereby each atom interacts with all the other atoms [Eq. (4.1)], which coincides with the analytical fit [Eq. (A10)].

peak appears at the shifted frequency $\delta = \delta_{LL}$ due to the Lorentz-Lorenz effect:

$$|\bar{\mathcal{E}}_{(p)}|_{\max}^2 = 1 + \delta_{LL}^2 = \frac{1}{|\bar{\mathcal{E}}_{(p)}|_{\min}^2}, \quad (3.6)$$

whose nature is essentially similar to, e.g., Lorentz-Lorenz resonance observed experimentally in alkali vapors [6]. However, in the 1D case considered here, the Lorentz-Lorenz shift and even its sign are polarization dependent. In particular,

$$(\delta_{LL})_{\parallel} = -Q_a S, \quad (\delta_{LL})_{\perp} = Q_a S/2, \quad (3.7)$$

i.e., the Lorentz-Lorenz resonance is redshifted for \parallel polarization of laser, and blueshifted for \perp polarization. The Lorentz field $\bar{\mathcal{E}}$ and Lorentz-Lorenz shift in the near-neighbor approximation [Eq. (3.3)] are determined by the same Eqs. (3.4)–(3.7), where one has to set $S=1$.

IV. SPATIALLY PERIODIC AND WAVE SOLUTIONS (LOCSITONS)

We look now for solution of Eq. (3.2) as the sum of *uniform* LF, $\bar{\mathcal{E}}$ [Eq. (3.4)] and oscillating ansatz $\Delta\mathcal{E} \propto \exp(\pm iqn)$, where q is an (unknown) wave number, similarly as in, e.g., the phonon theory [9], with the difference being that we have here an excitation of bound electrons, and not atomic vibrations. Essentially, the locsitons may be classified as *Frenkel* excitons [9] because of their no-electron-exchange nature.

The wave numbers q are found via the dispersion relation

$$D(q) \equiv \frac{1}{S} \sum_{n=1}^{\infty} \frac{\cos(nq)}{n^3} = \frac{\delta + i}{\delta_{LL}}. \quad (4.1)$$

The behavior of $D(q)$ in the lossless case, $\delta_{LL}^2 > \delta^2 \gg 1$, is depicted in Fig. 3 by the solid curve.

Within NNA, we have to set $S=1$ and replace the sum in Eq. (4.1) by its first term:

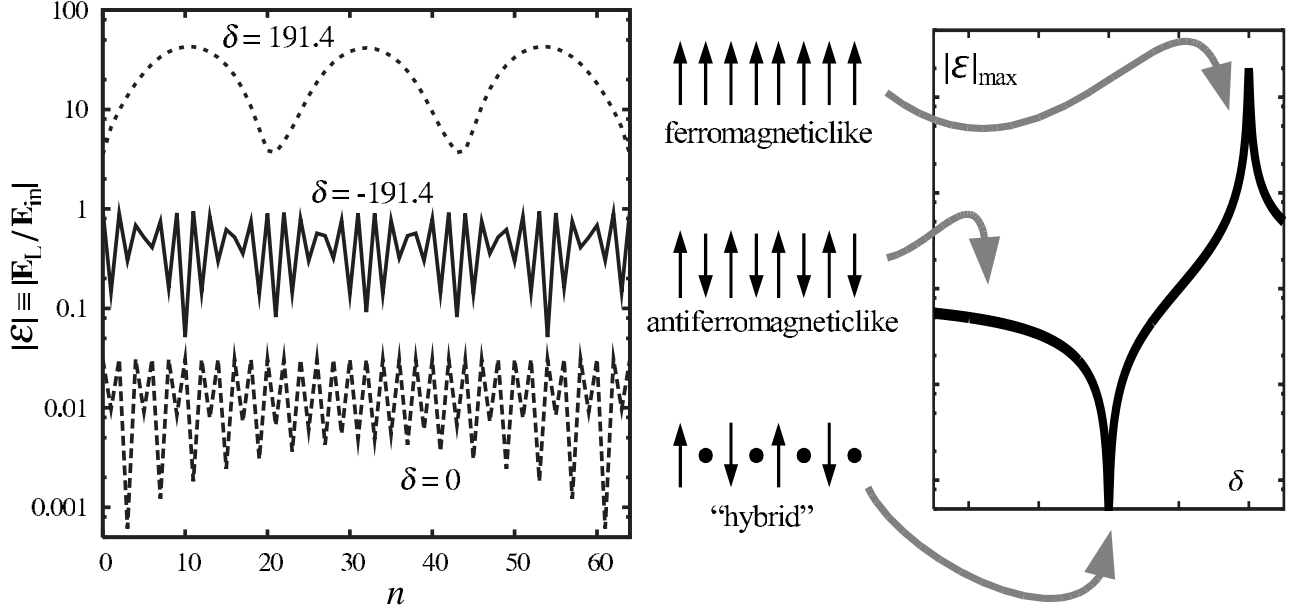


FIG. 4. Strata patterns of excitation and local field in finite arrays, and their relations to the resonance tuning in the case of 64 atoms and $\delta_{LL}=200$. Curves and patterns show long-wave ferromagneticlike excitation near the Lorentz-Lorenz resonance (top curve in the left plot and top pattern in the center), counterphase antiferromagneticlike excitation near the anti-Lorentz edge of the band (middle curve and pattern), and hybrid excitation near the point of atomic resonance (bottom curve and pattern). Note that all the curves in the left plot show *absolute* normalized amplitudes of the local field. Since the fields are in general complex, their absolute amplitudes are positive, so the near-zero points in the schematic depiction of the “hybrid” mode actually correspond to the lowest points of the bottom curve in the left plot.

$$D_{\text{NNA}}(q) \equiv \cos q = \frac{\delta + i}{\delta_{LL}} \quad (4.2)$$

(see Fig. 3, fine-dashed curve). Distinct oscillations emerge in the area between the two edges of the locsiton band. Their wave numbers are determined from Eq. (4.1) and (4.2) by neglecting the dissipation, i.e., by assuming real q and $\delta^2, \delta_{LL}^2 \gg 1$. One of the band edges corresponds to the maximum (and positive) $[D(q)]_{\text{max}}=1$ (same as for NNA, $[D_{\text{NNA}}(q)]_{\text{max}}=D(0)=1$), and thus to the Lorentz-Lorenz shift, $\delta = \delta_{LL}$. The other, “anti-Lorentz,” edge is at the opposite side of the atomic resonance, and is determined by the minimum (and negative) $D_{\text{min}}=D(\pi)$. Thus we have

$$\frac{\delta_{\text{anti}}}{\delta_{LL}} = \frac{D(\pi)}{D(0)}, \quad (4.3)$$

which can be evaluated using an amazingly simple relation for sum (4.1), which is actually valid for a more general sum and an arbitrary exponent $\rho > 1$:

$$\frac{D(\pi, \rho)}{D(0, \rho)} \equiv \frac{\sum_{n=1}^{\infty} (-1)^n n^{-\rho}}{\sum_{n=1}^{\infty} n^{-\rho}} = -1 + \frac{1}{2^{\rho-1}}. \quad (4.4)$$

This can be readily proven by an appropriate rearrangement of the terms in the sums in Eq. (4.4); see Eq. (A11). In the case of $\rho=3$ and infinite array [Eq. (4.1)], we have $\delta_{\text{anti}}/\delta_{LL}=-3/4$. Hence, the locsiton band is determined as

$$1 > \frac{\delta}{\delta_{LL}} > -\frac{3}{4} \quad \left(\text{or } \left| \frac{\delta}{\delta_{LL}} \right| < 1 \text{ within NNA} \right), \quad (4.5)$$

with well-developed locsitons at $\delta_{LL}^2 \gg 1$. Indeed, if the dissipation is neglected and the wave numbers q are real, there are an infinite number of solutions for them within limits (4.5). In this case the meaningful positive solutions, within the first Brillouin zone, are $-\pi \leq q < \pi$. The plots of the functions in the left-hand side of Eqs. (4.1) and (4.2) are shown as δ/δ_{LL} vs q in Fig. 3. Based on Eq. (4.5), the total width of the locsiton band in terms of δ is thus $(7/4)|\delta_{LL}|$, if one accounts for the interactions of each atom with *all* the rest of atoms in the infinite array, whereas it is $2|\delta_{LL}|$ in the near-neighbor approximation.

To gauge the dipole-dipole interaction in the lattice, one can also introduce its Rabi energy as

$$\hbar\Omega_R = \frac{\hbar Q_a}{T} = \frac{4|F_{(p)}||d_a|^2}{\epsilon l_a^3} \ll \hbar\omega_0. \quad (4.6)$$

It brings about a locsiton energy band of $\sim 2\hbar\Omega_R \gg \hbar\Gamma$ (if $\delta_{LL}^2 \gg 1$), akin to those in solid-state crystals [9], photonic crystals [10], and electronic bandpass filters.

One of the most interesting effects due to locsitons is a wide spectrum of the standing waves, strata, formed by them; see Fig. 4. As we already noted, they can range from the very long ones, LW strata, with the maximum spatial period being double of the whole length of a 1D array, similarly to the main mode of oscillation in a violin string, to SW strata whereby each dipole oscillates in counterphase to each

of its nearest neighbors. The latter mode is the strongest manifestation of the fact that the array of N atoms is a discrete-element resonator, akin to a string of beads connected to each other, with the beads capable of the same kind of motion, when each individual bead is oscillating in counterphase with its neighbor. Because in both cases the excitation is of dynamic nature and is due to external driving, the mechanical analogy of SW locsiton modes is more adequate than that of a static ferromagnetic configuration vs antiferromagnetic one; see also the Appendix.

It can be immediately found, e.g., from consideration of the plots in Fig. 4, upper curve, that the LW strata emerge at the laser tuning very near to the Lorentz-Lorenz resonance, i.e., in the limit $1 - \delta/\delta_{LL} \ll 1$. In this case, in both FIA (4.1) and NNA (4.2), the wave number q_{LW} and the respective spatial wavelength Λ_{LW} are

$$q_{LW} \approx \sqrt{1 - \left(\frac{\delta}{\delta_{LL}}\right)^2}, \quad \Lambda_{LW} = \frac{2\pi l_a}{q_{LW}}. \quad (4.7)$$

In the infinite array, the longest Λ is up to $2\pi l_a \delta_{LL}$, when $\delta_{LL}^2 - \delta^2 \sim 1$; the locsitons with longer wavelength get significantly suppressed.

The opposite limit, or the anti-Lorentz side of the locsiton band,

$$\frac{3}{4} + \frac{\delta}{\delta_{LL}} \ll 1 \quad \left(\text{for NNA it is } 1 + \frac{\delta}{\delta_{LL}} \ll 1 \right), \quad (4.8)$$

defines SW locsitons, with

$$q_{SW} \sim \pi, \quad \Lambda_{SW}/2 \sim l_a, \quad (4.9)$$

i.e., $\Lambda_{SW}/2$ is the finest grain of locsiton structure, as one would expect from the “bead-string” analogy. However, an incommensurability, i.e., mismatch between $\Lambda_{SW}/2$ and the lattice spacing l_a , whose ratio is in general an *irrational* number, results in a strong spatial modulation of the SW, giving rise to a *coarse* LW-like structure.

In the NNA, this coarse structure of SW mode has the half period roughly the same as for a pure LW mode, $\sim \Lambda_{LW}$. This can be readily understood in terms of “beating” between the locsiton wavelength, $2\pi/q$, and the spatial scale of the discrete structure of the system, which is the normalized spacing between atoms, 1. Indeed, near the anti-Lorentz edge, $\delta + \delta_{LL} \ll \delta_{LL}$, we can write for a SW wave number that $q_{SW} = \pi - \Delta q$, with $|\Delta q| \approx \sqrt{1 - (\delta/\delta_{LL})^2} = q_{LW}$, and find the spatial oscillations as

$$\mathcal{E}_n \propto \cos(nq_{SW}) = \cos(n\pi - n\Delta q) = (-1)^n \cos(n\Delta q), \quad (4.10)$$

with $\Delta q \approx q_{LW}$, which shows alternating, counterphase motion of the neighboring atoms, $(-1)^n$, modulated by a slow envelope, $\cos(nq_{LW})$. Both the fine grain and the coarse modulation may be well pronounced (Fig. 4, middle curve). At $q = \pi$, the LW and SW periods converge to the same scale, $4l_a$; see Eq. (4.12) below. Using the phonon analogy, the LW locsitons may be viewed to a certain extent as counterparts of acoustic phonons and SW locsitons as those of optical phonons.

Between those limiting points—LW locsitons at the Lorentz end of the locsiton spectrum, $\delta \sim \delta_{LL}$, and SW locsitons at the anti-Lorentz end, $\delta \sim -\delta_{LL}$ —there are all kinds of locsitons making chaotic looking strata (due to the above mentioned incommensurability, i.e., irrational ratio between a locsiton wavelength Λ and the array spacing l_a). However, same as in the chaotic motion, there are small islands of well-ordered wave patterns, located at the spectral points where the ratio Λ/l_a (or q/π) is a rational number, provided that the system is at a *resonance*; see Eqs. (5.2) and (5.3) below. One can think of them as sort of hybrids of ferromagneticlike and antiferromagneticlike behaviors. Indeed, the purely antiferromagneticlike SW locsiton at $q = \pi$ is formed by the atoms with alternating polarizations,

$$\cdots \uparrow \downarrow \uparrow \downarrow \uparrow \downarrow \cdots \quad \text{for } \perp \text{ polarization,}$$

$$\cdots \rightarrow \leftarrow \rightarrow \leftarrow \rightarrow \leftarrow \cdots \quad \text{for } \parallel \text{ polarization.}$$

$$(4.11)$$

This happens at $\delta \sim -\delta_{LL}$ within NNA and $\delta \sim -(3/4)\delta_{LL}$ for FIA. The simplest hybrid pattern is formed at $q = \pi/2$ (which is at $\delta = 0$ within NNA, and $\delta/\delta_{LL} = -3/32$ for a fully interacting array [Eq. (4.1)]), whereby each second atom is *non-excited*, while the other atoms alternate their polarization:

$$\cdots \uparrow \circ \downarrow \circ \uparrow \circ \downarrow \circ \uparrow \circ \downarrow \cdots \quad \text{for } \perp \text{ polarization,}$$

$$\cdots \rightarrow \circ \leftarrow \circ \rightarrow \circ \leftarrow \circ \rightarrow \circ \leftarrow \cdots \quad \text{for } \parallel \text{ polarization.}$$

$$(4.12)$$

Examples of other simplest hybrid states within NNA are $q = \pi/3$, $q = \pi/4$, etc. In general, periodic patterns exist if q/π is a rational number, i.e., for all the eigenresonances in finite 1D arrays within NNA; see Eq. (5.3) below.

Finally, it is worth noting that the strata, albeit fast decaying, exist even *beyond* the locsiton band [Eq. (4.5)]. They are not, however, propagating waves or locsitons, and their amplitudes exponentially decay with the distance. Consider the simplest case, NNA, with the losses negligibly small, $\delta^2 > \delta_{LL}^2 \gg 1$ in Eq. (4.2). In this case, $\cos^2 q > 1$ in Eq. (4.2), which indicates that the wave number q must be complex. Indeed, writing $q = -i\chi$ for the Lorentz end of the band, $\delta/\delta_L > 1$, and $q = -i\chi + \pi$ for the anti-Lorentz end, $\delta/\delta_L < -1$ (see also Sec. VI), we have the solution for χ as

$$\chi = \ln[|\delta/\delta_{LL}| \pm \sqrt{(\delta/\delta_{LL})^2 - 1}] \quad (4.13)$$

and for the local fields as

$$(\mathcal{E}_n)_{LL} \propto e^{\chi n} \quad \text{and} \quad (\mathcal{E}_n)_{antiLL} \propto e^{\chi n} (-1)^n \quad (4.14)$$

for the Lorentz and anti-Lorentz ends of the band, respectively. Here, in the case of a semi-infinite array, the sign in Eq. (4.13) has to be chosen such that the amplitude of the field vanishes at $|n| \rightarrow \infty$. These modes can be viewed as *evanescent locsitons*; see also Sec. VI. One can note though that they still bear the signature of the respective locsitons on either side of the band: long-wave, almost synchronous oscillations on the Lorentz end, and short-wave, phase-alternating oscillations on the anti-Lorentz end. In general, the same patterns hold in the FIA case.

V. QUANTIZATION OF LOCSITONS AND FIELD RESONANCES IN FINITE 1D ARRAYS

Due to boundary conditions in Eq. (3.1) [or Eq. (3.3) within NNA], the array of N atoms is a discrete-element resonator. This should result in locsiton quantization within the locsiton band [Eq. (4.5)] and corresponding size-related resonances of the local field. In a 1D array with N atoms, we have N coupled oscillators with the same individual atomic resonance frequency and, therefore, one should expect the original atomic line to be split into N lines at most, with the collective broadened band [Eq. (4.5)] being replaced with those lines. Of course, when the dissipation (or finite linewidth of each individual line) is taken into account, those split lines will merge into one continuous locsiton band [Eq. (4.5)] if the array is sufficiently large,

$$N > \frac{7}{4} |\delta_{LL}| \quad (\text{or } > 2 |\delta_{LL}| \text{ within NNA}). \quad (5.1)$$

The simplest result for the resonant line positions is obtained within NNA. Using boundary condition (3.3), i.e., $\mathcal{E}_0 = \mathcal{E}_{N+1} = 0$, we find that the longest locsiton half wave, corresponding to the fundamental mode, is

$$\Lambda_1/2 = (N+1)l_a, \quad q_1 = \pi/(N+1). \quad (5.2)$$

Thus, $\Lambda_1/2$ is the distance between nodes where LF zeros out, whereas the wavelengths Λ_k of eigenlocsitons and their eigenfrequencies δ_k , with the quantum number $1 \leq k \leq N$, are, respectively,

$$\begin{aligned} \Lambda_k &= \Lambda_1/k, & \delta_k &= \delta_{LL} \cos(q_k), \\ q_k &= \pi k/(N+1). \end{aligned} \quad (5.3)$$

[Note that the first Eq. (7) in Ref. [1], which corresponds to the second Eq. (5.3) here, contained a typo (an extraneous “ π ” in the cos argument) which we corrected here]. From these, only the resonances with odd k will be realized for a symmetric driving laser profile, in particular, the uniform one, $E_{in} = \text{const}$ (which is the most common case here), and with even k —for an antisymmetric one, say, $E_{in} = \text{const} \times (N+1-2n)/(N-1)$, where n is the sequence number of an atom in the array. In all other cases, a full set of N resonances will be realized.

In essence, the size-related locsiton resonances in discrete arrays are, to a limited extent, similar to any eigenresonances in regular continuous (i.e., nondiscrete) 1D system. Examples can be found both in classical setting, e.g., a violin string, a Fabry-Pérot resonator (such as, e.g., in a laser), and in quantum mechanics (QM), from the resonances in a quantum well with infinitely high walls, to electron gas in a finite layer [11], electrons in long molecules [12], etc. The major difference here is that the number of eigenmodes, or resonances, in an array with N elements is limited to N , in contrast to the theoretically infinite number of eigenmodes in continuous finite 1D systems.

The resonances for uniform driving within NNA are shown in Fig. 2 for $\delta_{LL} = 200$ in the cases of $N=12$ [Fig. 2(a)], $N=13$ [Fig. 2(b)], and $N=100$ [Fig. 2(c)]. One can readily find out that the lower amplitude envelope is

$$\mathcal{E}_{\min}(\delta) \approx 2|\bar{\mathcal{E}}|, \quad (5.4)$$

while the upper envelope of the resonant peaks within NNA for a uniform driving is

$$\mathcal{E}_{\max} \begin{cases} \approx |\bar{\mathcal{E}}|(n_\delta + n_\delta^{-1}) & \text{if } n_\delta \leq 1 \\ = 2|\bar{\mathcal{E}}| & \text{otherwise,} \end{cases} \quad (5.5)$$

where $n_\delta = (N+1)/(2\sqrt{\delta_{LL}^2 - \delta^2})$. As N increases, the resonances merge and are suppressed at $N = |\delta_{LL}|O(1)$; see, e.g., Fig. 2(c). However, even then \mathcal{E}_{\min} still exceeds the uniform field $|\bar{\mathcal{E}}|$ [Eq. (3.4)] by a factor of 2. For $N=3k-1$ (k is a natural number), LF amplitude dips below the lower envelope $|\mathcal{E}_{\max}|_{\text{low}}$ at $\delta = -\delta_{LL}/2$. At that frequency, within NNA, $\cos q' = -0.5$, $q' = 2\pi/3$, and the SW period $\Lambda = 3l_a$ is an integer of the atomic spacing, so only fine SW structure remains, resulting in an *antiresonance* and in the strongest inhibition of the locsiton.

VI. 1D ARRAYS BEYOND THE NEAR-NEIGHBOR APPROXIMATION

As we mentioned above, while the quantization of locsitons in finite arrays can be readily analyzed analytically within NNA (see the previous Secs. III and V) the situation with FIAs presents a challenge for an analytical treatment.

Let us briefly outline general analytical and numerical results obtained so far:

(a) A FIA locsiton band is not symmetric with respect to the atomic resonance, $\delta=0$. It is shorter by the factor of 3/4 on the anti-Lorentz side [see Eq. (4.5)], in contrast to the NNA.

(b) Respectively, FIA resonances are grouped tighter on the anti-Lorentz side of the band, albeit their number is the same as for NNA. Near the Lorentz side of the band, the NNA-predicted resonances coincide more closely with those obtained by FIA numerical calculations.

The major source of these effects is the first factor, i.e., a strongly asymmetric (with respect to the detuning frequency δ) shape of the dispersion relation (Fig. 3). A more detailed mathematical consideration of this problem, including a very good *analytical* fit for the dispersion relation, is found in the Appendix. Less significant, although interesting as far as the eigenmodes of 1D arrays are concerned, is the fact that simple NNA eigen-wave-numbers [Eq. (5.3)], $q_k = \pi k/(N+1)$, obtained based on the NNA boundary conditions $\mathcal{E}_0 = \mathcal{E}_{N+1} = 0$ [Eq. (3.3)] are not exact anymore. One has to use now more extended, “beyond-the-boundary” conditions [Eq. (3.1)], which are the signature of FIA, whereby

$$\mathcal{E}_n = 0 \quad \text{for all } n < 1 \text{ and } n > N, \quad (6.1)$$

instead of just two end points in NNA. To explore the problem, let us simplify it first by considering only nondissipating atoms, $\delta_{LL}^2 \geq \delta^2 \gg 1$, and rewrite full-interaction dispersion relation (4.1) for this case as

$$\frac{1}{S} \sum_{n=1}^{\infty} \frac{\cos(nq)}{n^3} = D(q) \equiv \frac{\delta}{\delta_{LL}}, \quad (6.2)$$

assuming $D(q)$ to be real. The equation for the field is written then as

$$\mathcal{E}_n - \frac{1}{D} \sum_{\substack{j \neq n \\ -\infty \leq j \leq \infty}} \frac{\mathcal{E}_j/2S}{|j-n|^3} = 1, \quad (6.3)$$

with boundary conditions (6.1).

The plot $D(q)$ for real q 's due to dispersion relation (6.2) is shown in Fig. 3 with the solid curve. The new qualitative difference now between FIA [Eq. (6.2)] and the NNA case [Eq. (4.2)] without dissipation, i.e., $\cos q = D$, is as follows. With $D^2 \leq 1$, the NNA equation has *only real* solutions for q , whereas Eq. (6.2), even within the locsiton band, $-3/4 \leq D \leq 1$, aside from real solution for $q \equiv \tilde{q}$, has, as one can show, an *infinite* number of *complex* solutions q for *each* single real solution \tilde{q} (i.e., for the same D). All of them, in addition to fast spatial oscillation terms, have a rapidly rising or falling exponential factor. These exponential modes are negligibly small almost over the entire array length if $N \gg 1$, and they need to be accounted for only very near the end points of the array, where they are instrumental in zeroing out the field and excitation at the points $n < 1$ and $n > N$.

Let us illustrate the formation of those exponential (or *evanescent*) modes and their role in boundary conditions for the 2-NNA, whereby field equation (6.3) becomes

$$\mathcal{E}_n - \frac{9}{4D} \left[(\mathcal{E}_{n-1} + \mathcal{E}_{n+1}) + \frac{1}{8} (\mathcal{E}_{n-2} + \mathcal{E}_{n+2}) \right] = 1, \quad (6.4)$$

with the boundary conditions for *two* pairs of end points:

$$\mathcal{E}_n = 0 \quad \text{at } n = 0, -1 \text{ and } n = N + 1, N + 2. \quad (6.5)$$

The dispersion relations approximating Eq. (6.2) will read now as

$$\frac{8}{9} \left[\cos q + \frac{\cos(2q)}{8} \right] = D(q) \quad (6.6)$$

(see Fig. 3, long-dashed curve), and the locsiton band is determined by

$$-7/9 \leq D(q) \leq 1. \quad (6.7)$$

The real solutions \tilde{q} of Eq. (6.6) are those for which $\cos^2 \tilde{q} \leq 1$; they give rise to strata modes of Eq. (6.4),

$$\mathcal{E}_n \propto \exp(\pm i\tilde{q}n). \quad (6.8)$$

However, having in mind that $\cos(2q) = 2 \cos^2 q - 1$, one can readily see that Eq. (6.6) has also solutions with $\cos^2 q > 1$, i.e., those that correspond to exponential modes, with complex $q = q_{\text{evn}2}$. Introducing for those modes

$$q_{\text{evn}2} = -i\chi + \pi \quad (6.9)$$

with real χ , we obtain from Eq. (6.6) that for each given real \tilde{q} the exponent χ is determined by

$$\cosh \chi = 4 + \cos \tilde{q}, \quad (6.10)$$

and the respective exponential mode is

$$(\mathcal{E}_n)_2 = e^{\pm(\chi+i\pi)n} = e^{\pm\chi n} (-1)^n. \quad (6.11)$$

Thus, these 2-NNA modes are antiferromagneticlike strata, modulated by fast exponents. Indeed, since $3 \leq \cosh \chi \leq 5$, we have $1.76 < \chi < 2.3$.

Since the exponential, or evanescent, modes have so short "tails," they produce relatively small correction for the respective eigenwavelengths Λ_n and for q_n , compared to the NNA oscillatory modes, Eqs. (5.2) and (5.3), so that we can look for the Λ_n corrected for 2-NNA at the points of resonances as

$$\frac{\Lambda_k}{2l_a} = \frac{N+1+\Delta_k}{k}, \quad \Delta_k = O(1),$$

$$\tilde{q}_k = \pi \frac{2l_a}{\Lambda_k}, \quad (6.12)$$

with the correction $\Delta_k > 0$, similarly to, e.g., oscillations in a violin string with a "soft" suspension at its ends. To find Δ_k of the k th resonance, we seek a solution for \mathcal{E}_n as a sum of two modes: oscillatory and exponential ones. Then, for symmetric modes, i.e., with odd k , we have a full solution written as

$$(\mathcal{E}_n)_{\text{odd}} = \cos(\tilde{q}_k \bar{n}) + C \cosh[\chi(\tilde{q}_k \bar{n})] (-1)^n,$$

$$\bar{n} = n - \frac{N+1}{2}, \quad (6.13)$$

where C is a constant. For antisymmetric modes, with even k , we have

$$(\mathcal{E}_n)_{\text{even}} = \sin(\tilde{q}_k \bar{n}) + C \sinh[\chi(\tilde{q}_k \bar{n})] (-1)^n. \quad (6.14)$$

Using now conditions (6.5), we can write for the points $n = -1$ and $n = 0$, respectively, the following equations for symmetric modes (6.13):

$$(\mathcal{E}_{-1})_{\text{odd}} = \cos\left(\frac{\pi k}{2} \frac{N+3}{N+1+\Delta_k}\right) - C \cosh\left(\chi \frac{N+3}{2}\right) = 0, \quad (6.15)$$

$$(\mathcal{E}_0)_{\text{odd}} = \cos\left(\frac{\pi k}{2} \frac{N+1}{N+1+\Delta_k}\right) + C \cosh\left(\chi \frac{N+1}{2}\right) = 0. \quad (6.16)$$

For antisymmetric modes (6.14), one has to replace cosine and hyperbolic cosine functions in Eqs. (6.15) and (6.16) with sine and hyperbolic sine functions, respectively. From these two equations we can compute Δ_k and C . Indeed, approximating $\cosh(\xi) \approx \sinh(\xi) \approx e^{\xi}/2$ in Eqs. (6.15) and (6.16) or in the respective equations for antisymmetric modes, since $\chi(N+1) \gg 1$, we obtain two equations for Δ_k and C , which are readily solved for Δ_k and C for *both* symmetric and antisymmetric modes as

$$\Delta_k = \frac{2}{q_{\text{NNA}}} \tan^{-1} \left[\frac{\sin(q_{\text{NNA}})}{e^{\chi} + \cos(q_{\text{NNA}})} \right],$$

$$q_{\text{NNA}} = \frac{\pi k}{N+1} \quad (6.17)$$

and

$$C = q_{\text{NNA}} \Delta_k (-1)^{\bar{k}/2} e^{-\chi(N+1)}, \quad (6.18)$$

where from Eq. (6.10), $\chi \approx \cosh^{-1}[4 + \cos(q_{\text{NNA}})]$, while $\bar{k} = k+1$ for symmetric modes, and $\bar{k} = k$ for the antisymmetric ones. It is worth noting that boundary conditions (6.5) at $n = N+1, N+2$ are now satisfied automatically because of our choice of the coordinate \bar{n} in Eqs. (6.13) and (6.14). For LW resonances, $k \ll N$, Eq. (6.17) reduces to

$$\Delta_k \approx \frac{2}{e^\chi + 1} \approx \Delta_{\text{max}} \approx \frac{2}{11}, \quad (6.19)$$

which is the maximum magnitude of Δ_k , whereas for SW resonances, $N+1-k \ll N+1$, Eq. (6.17) reduces to

$$\Delta_k \approx \frac{2}{e^\chi - 1} \left(\frac{N+1}{k} - 1 \right) \approx \frac{2}{5} \left(\frac{N+1}{k} - 1 \right), \quad (6.20)$$

which is substantially smaller than LW correction (6.19). One can readily see that Δ_k is a monotonically decreasing function of k . In the middle of the locsiton band, $k \sim (N+1)/2$, we have

$$\Delta_k \approx \frac{4}{\pi e^\chi} \approx \frac{1}{2\pi}. \quad (6.21)$$

Interestingly, a fairly good fit to Eq. (6.17) is provided by a much simpler formula:

$$\Delta_k \approx \Delta_{\text{max}} \left[1 - \left(\frac{k}{N+1} \right)^3 \right]. \quad (6.22)$$

Now, once the correction Δ_k is found, one can substitute $q = \tilde{q}_k = \pi k / (N+1 + \Delta_k)$ [Eq. (6.12)] into dispersion relation (6.6) and calculate the respective frequency detuning for the k th resonance, $D_k = \delta_k / \delta_L$, with $k=1$ being the closest to the Lorentz-Lorenz resonance, i.e., a LW mode, and $k=N$ closest to the anti-Lorentz edge of the locsiton band, a SW mode.

A way to extend the 2-NNA approximation to a full-array interaction is to apply result (6.17) for the correction of the eigen-wave-number \tilde{q}_k , but use it now in the full-blown dispersion relation (6.2), instead of 2-NNA relation (6.6), to calculate the resonance detuning δ_k . The other avenue, of course, is to seek for higher-order approximations. For example, one can take into account two edge sets of *three points* each, i.e., similarly as for Eq. (6.5), stipulate 3-NNA:

$$\mathcal{E}_n = 0 \quad \text{at } n = 0, -1, -2$$

and

$$n = N+1, N+2, N+3. \quad (6.23)$$

Following the same route as for 2-NNA case, we obtain now, similarly as for Eq. (6.10), a *second-order* equation for the *exponential eigenmode* complex wave number $q = q_{\text{evn}3}$ for any given oscillation wave number \tilde{q} as

$$16 \cos^2 q + \cos q (16 \cos \tilde{q} + 27) + (104 + 16 \cos^2 \tilde{q} + 27 \cos \tilde{q}) = 0 \quad (6.24)$$

[we leave it untransformed to $\cosh \chi$, unlike Eqs. (6.9) and (6.10), since in 3-NNA case the solution becomes more complicated than Eq. (6.11), and that transformation does not simplify the problem.] The higher-order equation for the *exponential eigenmodes* ensue the choice of a higher number of end points in the boundary conditions.

It has to be noted, however, that for specifying parameters of oscillating eigenmodes, the increase in the precision by accounting for higher-order exponential modes is of very limited, if purely academic, significance. Essentially, for large arrays, $N \gg 1$, the combination of the NNA for predicting the wave numbers \tilde{q} [Eq. (6.12) and (5.3)], with these \tilde{q} 's used then in Eq. (6.2) to calculate the resonance eigenfrequencies δ , does already a good job. A further step in increasing the precision provided by the 2-NNA corrections to eigen-wave-numbers is to again use the corrected \tilde{q} 's in Eq. (6.2) for the same purpose, and it is more than sufficient. A special case is a small array, e.g., $N=2, 3, 4$, whereby it is actually preferable to simply solve the general 1D-array equations analytically, similarly as in [1] in the case of $N=2$.

VII. MAGIC NUMBERS

A fundamental effect of self-induced cancellation of local-field suppression emerges near the atomic resonance, $\delta=0$, at certain magic numbers N . If $\delta_{\text{LL}}^2 \gg 1$, the *uniform* (Lorentz-Lorenz) LF (3.4) at $\delta=0$ is very small, $|\mathcal{E}| \sim |\delta_{\text{LL}}|^{-1}$ [Eq. (3.5)]. However, in the near-neighbor approximation, if

$$N = km_{\text{mag}} + 1, \quad m = 1, 2, 3, \dots, \quad (7.1)$$

where $m_{\text{mag}}=4$ is a magic number within NNA, locsitions at $\delta=0$ show canceled LF suppression at some atoms. The highest cancellation is attained at $\delta=0$ and $N=5$, with the atomic dipoles lining up as in Eq. (4.12), whereby the LF amplitude at odd-numbered atoms is at maximum, $|\mathcal{E}_{\text{max}}| \approx 1/3$, and the enhancement $|\mathcal{E}_{\text{max}}/\bar{\mathcal{E}}|_{\text{enh}}^2 \approx \delta_{\text{LL}}^2/9$ could be a few orders of magnitude. The LF at the two other atoms almost zeros out.

The self-induced cancellation effect is produced by a standing wave with the nodes at atoms with even numbers. This results in a “virtual” size-related resonance at $\delta \rightarrow 0$ (i.e., at the exact atomic resonance), which manifests itself in the enhancement (the resonant peak transpires in $|\mathcal{E}_{\text{max}}/\bar{\mathcal{E}}|$ vs δ). Thus, the nature of magic numbers is the *coincidence* of the atomic resonance with one of the size-related locsiton resonances.

The effect holds also for the interaction of each atom with *all* other atoms [Eq. (3.1)]. The magic number in Eq. (7.1) takes on a “devilish” likeness here: $m_{\text{mag}}=13$. It is due to the fact that for $\delta=0$ and $\delta_{\text{LL}} \gg 1$, the first root q' of Eq. (4.1) with zero right-hand side (rhs),

$$\sum_{n=1}^{\infty} \frac{\cos(nq')}{n^3} = 0, \quad (7.2)$$

has its property of q'/π almost coinciding with a rational number, $q'/\pi \approx 6/13$ ($13q'/6\pi = 1.000\ 26\cdots$); see the Appendix. The locsiton wavelength is $\Lambda = 2\pi/q' = (13/3)l_a$, and the lowest integer of $\Lambda/2$ to exactly match an integer of l_a is $13l_a$, which requires 14 atoms. We have now $|\mathcal{E}_{\max}| \approx 2/15$, with enhancement of $\sim 4\delta_{\text{LL}}^2/225$.

As we showed in [1], 2D lattices can also exhibit “magic shapes” with similar properties. The simplest one within NNA is a six-point star with an atom at its center, thus making the total number of atoms again $N=13$. More details on magic shapes for 2D lattices will be discussed by us elsewhere.

VIII. TRAVELING LOCSITON WAVES: VELOCITY AND PENETRATION DEPTH

If the locsitons are waves, can they be excited outside the driving field area, and thus travel away from the Lorentz-Lorenz uniform local-field area? How far can they travel before being extinguished? How fast do they propagate? Having in mind their dissipation, what is the size of a finite array to have well-pronounced standing waves and size-related resonances?

Of course, the locsitons can propagate in an array even in the areas inaccessible for the external (laser) field. If the spatial profile gradient of the driving wave is large enough, a LF excitation can be found beyond the driving field area. The terminological irony here is that the *local*-field phenomenon is due to a *nonlocal* interaction, and the locsitons can propagate away from their origination point. This may happen when the external laser field is nonuniform and has a large gradient, e.g., when one entirely screens out a part of the array by imposing a “sharp knife” over the array.

Even simpler and more transparent case is when only an end point of a semi-infinite 1D array [say, with $n=1$ in Eq. (3.1)] is illuminated by a laser field via a pinhole. Equation (3.1) has then nonzero (unity) rhs for $n=1$ only, and the rhs zeroes out at all the other points. In this case, *no* Lorentz-Lorenz local field exists for any atom at $n > 1$, and the only field and atomic excitation passed along the array of atoms will be locsitons. This may be the best way to excite and observe “pure” locsitons, with them not being masked by any external, averaged, mean, etc., fields. With such an arrangement, the 1D array (or a sufficiently thin atomic “cylinder” or carbon nanotube) becomes a true and effective waveguide for locsitons, capable of transmitting nondiffracting radiation and atomic excitation from one location (e.g., in optoelectronic circuits) to another.

The main issue here is how far the locsiton can propagate. One can investigate it by studying dispersion relation (4.1) and (4.2), which predicts not only the locsiton wave numbers, $q' \equiv \text{Re}(q)$, for any given frequency detuning δ , but also their dissipation depth or distance (in terms of numbers of atoms) for each wave number as $N_{\text{dis}} = 1/q''$, where $q'' \equiv \text{Im}(q)$. Using only the NNA dispersion relation (4.2), sufficient here, since the calculation of the dissipation distance

does not require the same precision as for the real wave numbers, we find out that the exact solutions for q' and q'' are determined by

$$\cos^2(q') = \frac{1}{2} \left(1 + \frac{\delta^2 + 1}{\delta_{\text{LL}}^2} \right) - \sqrt{\frac{1}{4} \left(1 + \frac{\delta^2 + 1}{\delta_{\text{LL}}^2} \right)^2 - \frac{1}{\delta_{\text{LL}}^2}} \quad (8.1)$$

and

$$\sinh^2(q'') = -\frac{1}{2} \left(1 - \frac{\delta^2 + 1}{\delta_{\text{LL}}^2} \right) + \sqrt{\frac{1}{4} \left(1 - \frac{\delta^2 + 1}{\delta_{\text{LL}}^2} \right)^2 + \frac{1}{\delta_{\text{LL}}^2}}. \quad (8.2)$$

From Eq. (8.1), for very small dissipation, i.e., when $\delta_{\text{LL}}^2 > \delta^2 \gg 1$, we have, as expected,

$$\cos(q') \approx \frac{\delta}{\delta_{\text{LL}}}. \quad (8.3)$$

The dissipation length in terms of the numbers of atoms, $N_{\text{dis}} = 1/q''$, is readily found from Eq. (8.2). At the exact atomic resonance, $\delta=0$, if $\delta_{\text{LL}}^2 \gg 1$, we have

$$q'' \approx \frac{1}{|\delta_{\text{LL}}|}, \quad N_{\text{dis}} \approx |\delta_{\text{LL}}|. \quad (8.4)$$

In general, in the most part of the locsiton band (except for the edge areas, $\delta_{\text{LL}}^2 - \delta^2 \lesssim 1$), we find that

$$q'' \approx \frac{1}{\sqrt{\delta_{\text{LL}}^2 - \delta^2}}, \quad N_{\text{dis}} \approx \sqrt{\delta_{\text{LL}}^2 - \delta^2}. \quad (8.5)$$

Finally, at the locsiton band edges, defined as $\delta_{\text{LL}}^2 - \delta^2 = 1$, Eq. (8.2) results in

$$q'' \approx \frac{1}{\sqrt{\delta_{\text{LL}}}}, \quad N_{\text{dis}} \approx \sqrt{\delta_{\text{LL}}}, \quad (8.6)$$

and it remains roughly the same as δ^2 reaches δ_{LL}^2 .

Thus, in the most of the locsiton band, the dissipation length, in terms of the numbers of atoms, is $N_{\text{dis}} = O(\delta_{\text{LL}})$, which also determines the maximum size of array to still enable the size-related resonances, in agreement with Sec. V.

Let us address now the characteristic velocities of the locsitons. Neglecting decay in Eq. (4.2) ($\delta_{\text{LL}}^2 > \delta^2 \gg 1$), the group velocity of locsitons, $v_{\text{gr}} = l_a(d\omega/dq)$, is found as

$$v_{\text{gr}} = \frac{l_a d\delta}{T dq}, \quad \cos q = \frac{\delta}{\delta_{\text{LL}}}. \quad (8.7)$$

Hence

$$\frac{dq}{d\delta} = -\frac{1}{\sqrt{\delta_{\text{LL}}^2 - \delta^2}},$$

$$v_{\text{gr}} = l_a \sqrt{\Omega_{\text{R}}^2 - \Delta\omega^2} = v_{\text{R}} \sqrt{\delta_{\text{LL}}^2 - \delta^2}, \quad (8.8)$$

where Ω_{R} is the Rabi frequency of the self-interacting array [Eq. (4.6)], and $v_{\text{R}} = \Omega_{\text{R}} l_a$ is a characteristic Rabi speed,

$$\frac{v_R}{c} = \alpha \left| \frac{d_a}{el_a} \right|^2 O(1) \ll 1, \quad (8.9)$$

which could be even slower than the typical speed of sound in condensed matter. This effect can be used, e.g., for developing nanosize delay lines in molecular computers and in optical gyroscopes. The LW-locciton phase velocity is

$$v_{\text{ph}} \approx \frac{v_R^2}{v_{\text{gr}}}. \quad (8.10)$$

IX. NONLINEAR EXCITATION OF A 1D ARRAY: OPTICAL BISTABILITY AND HYSTERESIS

So far we studied linear (in field) excitations of atomic 1D arrays. The nonlinear interactions open a door to a huge landscape of effects. The simplest and very generic nonlinearity in a two-level system is the saturation of its absorption [Eqs. (2.4) and (2.5)], which translates into a nonlinear response of the atom polarization to the local field [Eq. (2.6)]. This, in turn, nonlinearly affects the strength of interaction between atoms [Eq. (2.9)]. This represents a rare case whereby the nonlinear change (decrease) in absorption directly affects the eigenfrequencies of the system (1D array), by directly reducing the interaction. Many nonlinear effects are brought up in short pulse modes, e.g., discrete solitons, to be considered by us elsewhere. However, spectacular effects, such as hysteresis and optical bistability, emerge even in cw mode.

To write a set of nonlinear equations for an infinite 1D array, we first scale all fields to the characteristic saturation field E_{sat} [Eq. (2.5)], instead of scaling to the incident field E_{in} , so that the dimensionless local fields at the n th atom, Y_n , and the incident field X are

$$X = E_{\text{in}}/E_{\text{sat}}, \quad Y_n = E_n/E_{\text{sat}}, \quad (9.1)$$

and the nonlinear counterpart of Eqs. (3.1) and (3.2) for the array is written now as

$$Y_n - \delta_{\text{LL}}(\delta - i) \sum_{\text{latt}}^{j \neq n} \frac{Y_j/2S}{|j-n|^3(1 + \delta^2 + |Y_j|^2)} = X, \quad (9.2)$$

where δ_{LL} is defined by Eq. (3.4), so it covers either incident polarization. The nonlinear counterpart of NNA-based Eq. (3.3) is now

$$Y_n - \frac{\delta_{\text{LL}}(\delta - i)}{2} \left(\frac{Y_{n-1}}{1 + \delta^2 + |Y_{n-1}|^2} + \frac{Y_{n+1}}{1 + \delta^2 + |Y_{n+1}|^2} \right) = X, \quad (9.3)$$

$$\mathcal{E}_0 = \mathcal{E}_{N+1} = 0.$$

None of this is an easy object even for numerical solution, let alone analytical one. We have, however, derived in [1] a closed analytical solution for the nonlinear mode in the most fundamental system—an array of just two atoms—and found bistability and hystereses in such a mode. In this paper, more as a matter of illustration, we find an analytical multistable solution and hysteresis for the simplest case of Lorentz-Lorenz uniform field. However, our computer simulations

showed that multistability and hystereses exist in the vicinity of each size-related resonance in the system.

For the sake of simplicity, we consider here the case of Lorentz-Lorenz uniform mode. In near-neighbor approximation (9.3) [the FIA results will essentially differ only by a factor of $O(1)$], we have $Y_n = Y_{n-1} = Y_{n+1} \equiv Y$. Thus the nonlinear equation for the uniform local field Y is

$$Y \left[1 - \frac{\delta_{\text{LL}}(\delta - i)}{1 + \delta^2 + |Y|^2} \right] = X, \quad (9.4)$$

or for the field intensity $|Y|^2 \equiv y$,

$$y \frac{[1 - \delta(\delta_{\text{LL}} - \delta) + y]^2 + \delta_{\text{LL}}^2}{(1 + \delta^2 + y)^2} = X^2. \quad (9.5)$$

It can be readily seen that the strongest nonlinear effect emerges near the Lorentz-Lorenz resonance, $\delta \approx \delta_{\text{LL}}$. Assuming small losses, $\delta, \delta_{\text{LL}} \gg 1$, we can analyze the threshold of the multistability and hysteresis mode by stipulating that $y \ll \delta_{\text{LL}}^2$ and $\Delta \equiv \delta_{\text{LL}} - \delta \ll \delta_{\text{LL}}$. Thus Eq. (9.5) can be further simplified as

$$y[(y - \delta_{\text{LL}}\Delta)^2 + \delta_{\text{LL}}^2]/\delta_{\text{LL}}^4 \approx X^2. \quad (9.6)$$

The threshold for the multistable solution $y(X)$ of this equation is determined by the condition $dX/dy = d^2X/dy^2 = 0$, which results in the critical requirement that

$$\Delta \equiv \delta_{\text{LL}} - \delta > \Delta_{\text{cr}} = \sqrt{3},$$

$$y \equiv |Y|^2 > y_{\text{cr}} = \frac{2}{\sqrt{3}} \delta_{\text{LL}},$$

$$X^2 > X_{\text{cr}}^2 = \frac{1}{\delta_{\text{LL}}^2} \left(\frac{2}{\sqrt{3}} \right)^3. \quad (9.7)$$

Amazingly, as one recalls that $X = E_{\text{in}}/E_{\text{sat}}$ and $\delta_{\text{LL}} \gg 1$, the critical (threshold) driving intensity E_{in}^2 to initiate multistability and hysteresis could be orders of magnitude lower than the saturation one, E_{sat}^2 , which is mostly due to resonant nature of the effect that emerge in the vicinity of the Lorentz-Lorenz resonance. Thus, the required saturation nonlinearity is indeed just a slight perturbation to the resonant linear mode. This should be of no big surprise, since the nature of the effect is the same as in many other so-called *vibrational hystereses* [13] in resonant nonlinear systems, from pendulum [13] to electronic circuits [14], to optical bistability in a Fabry-Pérot resonator [15], to a cyclotron resonance of a slightly relativistic electron [16]. In all these nonlinear resonances, it is enough for a narrow resonant curve to be tilted beyond its resonance width to reach multistability by becoming “Pisa-type tower.”

The formation of bistability and hysteresis is depicted in Fig. 5, where the resonant curve $Y(\delta)$ is shown for different driving X 's for the full Eq. (9.5). The formation of a tristable solution results in the so-called bistability, whereby only the states with the maximum and minimum intensities are stable, whereas the middle branch of the solution is absolutely unstable. To an extent, it is similar to one of the hysteretic patterns for the local field found for the case of the local field

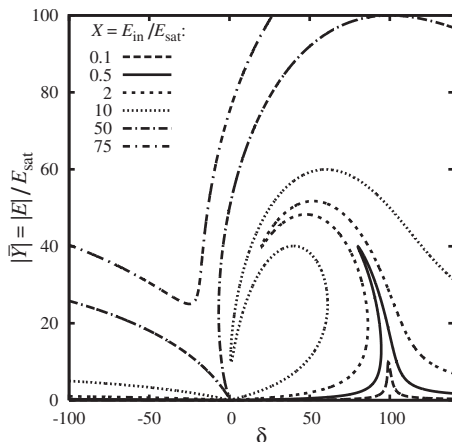


FIG. 5. Multistability of Lorentz-Lorenz mode in a long array: local Lorentz field amplitude Y vs detuning δ for different normalized driving amplitudes $X = E_{in}/E_{sat}$ for the case of $\delta_{LL} = 100$.

[1] and scattered light [17] of just two atoms. The hysteretic resonance here is produced by a Lorentz-type, or ferromagneticlike, excitation of atoms with LW locsitions. This effect is also reminiscent of optical intrinsic bistability for uniform LF in dense materials predicted earlier in [18] and observed experimentally in [19].

The above result for hysteresis and bistability was found for the uniform, Lorentz, field, i.e., near the Lorentz-Lorenz resonance, using a simple field distribution. However, it is clear from the above argument that with a Pisa-type tower, a similar hysteretic effect can be expected in the close vicinity of every size-related locsiton resonance within the locsiton band. Some of the most interesting hystereses, though, are excited for the SW locsitions, when the nearest atoms counteroscillate in an antiferromagneticlike fashion, as shown in [1] for the anti-Lorentz band edge for two atoms. This hysteresis results in a “split-fork” bistability and will be discussed by us in application to long arrays elsewhere.

X. ANALOGIES TO LOCSITONS IN OTHER PHYSICAL SYSTEMS AND GENERAL DISCUSSION

It is only natural to expect the effects studied here to manifest themselves in other finite systems of discrete resonant oscillators that are externally driven and interact with each other. On one hand, this may help to demonstrate and verify some major results reported here in much simpler and easily handled settings. On the other hand, this may bring up new features in these other systems that escaped attention in seemingly well-developed and researched fields. We consider here a few such systems.

Perhaps, the most classical example would be a mechanical finite array of identical physical pendulums with the same individual resonant frequencies, weakly coupled to each other (say, by using weak strings between neighboring pendulums), with each pendulum driven independently by an external feed (say, via EM solenoids) with the same phase for all of them. By tuning the frequency of the driving feed around the resonant frequency of the pendulums, one may expect to observe stratified excitation of the pendulums, from

long-wave, ferromagneticlike strata to short-wave, antiferromagneticlike ones. One can also expect to observe magic numbers and related effect of nonmoving pendulums surrounded by strongly excited ones. (It is worth noting that we are talking here about a cw motion, in contrast to the well-known effect in two coupled nondriven pendulums, whereby the pendulums periodically alternate periods of zero excitation in one and strong excitation in the other one, with the frequency of the alternation being inversely proportional to the coupling.) The major effect here would be again due to locsitions, and the major critical condition for their excitation would be similar to the condition on the strength of interaction, Q_a [Eq. (2.10)], to exceed a critical one.

The driven pendulum array would be a great classroom-demonstration tool. However, although purely mechanical, it might take some effort to implement, due to the need of an independent feed to each pendulum. From that point of view, a much simpler, easily implementable, controllable, recordable, and versatile system could be an electronic array of individual resonant circuits, electronically coupled to each other. A long while ago, similar systems have been used as transmission lines, whereas a finite set of circuits has also been of interest for such applications as bandpass filters. However, the detailed picture of behavior of individual circuits inside such systems has apparently not attracted too much attention, with a few reasons for that. The main difference between these systems and the ones proposed by us is that we need an independent feed with the same phase for each individual circuit, which may be arranged by, e.g., using individual cable for each one of them. The coupling between the individual circuits can be engineered in such a way that one can arrange strictly near-neighbor interaction, two-near-neighbors interaction, etc. Moreover, the contribution of each neighboring circuit can be independently controlled, so the term $1/n^3$ can now be changed to any desirable function of the neighbor spacing.

A close example, which might have important implications for large radio-frequency antenna arrays, for example, radio-astronomy applications, as well as in multidish radar systems, is the interaction of radiators in those arrays, if the strength of this interaction exceeds some critical value.

Since in the case of electronic circuits the polarization of the feed and the spatial anisotropy as in Eq. (2.2) is not a factor anymore, the dipolelike interaction is simplified, as its spatial polarization form factor $F_{(p)}$ (as in Sec. III) can be now dropped, and equations of motion (3.1)–(3.4) can be simplified. Furthermore, since now the direction of a “dipole” with respect to the “incident polarization” is not a factor, one can arrange a *loop* or *ring* of those circuits, instead of a linear 1D array, which allows for periodic boundary condition instead of zero boundary conditions such as, e.g., in Eq. (3.1). This would greatly simplify the theory and comparison with the experiment, on one hand, and allow for interesting effects in ring arrays (such as, e.g., greatly enhanced Sagnac effect and related gyroscope applications), to be discussed by us elsewhere, on the other hand.

An interesting and exotic opportunity with 1D arrays, and especially ring arrays, is the possibility of developing a toy model of “discrete-space quantum mechanics (QM),” whereby a wave function is replaced by a set of oscillating

fields at discrete spatial points, instead of a regular wave distributed in space. This discrete-space QM could be of interest for the theory of certain systems, as well as from fundamental point of view. For example, the ring arrays then would allow building of a theory of a Bohr-type “discrete-QM H atom,” with finite number of primary quantum numbers, unlike an infinite numbers of quantum levels as in a regular-QM H atom.

A very interesting analogy, especially from the application point of view, is *magnetic spin resonance*, in particular *nuclear magnetic resonance* (NMR) [20], as well as magnetic resonances in finite spin systems, in particular so-called molecular magnets [21]. They have some common points with the interacting systems considered here, in particular, two-level nature of resonances in both systems.

In optical domain, an observation of the effect discussed here can be done in a few ways. Nanostrata and locsitions can be observed either via size-related resonances in scattering of laser radiation, or via x-ray or electron-energy-loss spectroscopy of the strata.

The effect has promising potential for molecular computers [22] and nanodevices. The major advantage of locsitions vs electrons in semiconductors is that they are not based on electric current or charge transfer. This may allow for a drastic reduction in the size limit for computer logic elements currently based on metal-oxide-semiconductor technology, which may suffer from many irreparable problems on a scale below 10 nm. As such, locsiton-based devices could be an interesting entry into the field, as complementary or alternative to emerging technologies such as plasmonics [23] or spintronics [24]. They can offer both passive (e.g., transmission lines and delays) and active elements, e.g., for switching and logics. A ring array may be used as a basis for a Sagnac-locsiton-based gyroscope; low locsiton velocity may allow for a high sensitivity in a small ring.

Another promising application of locsitions could be biosensing devices, where target-specific receptor molecules either form a locsiton-supporting lattice or are attached to its sites. A localized locsiton occurs whenever a target biomolecule attaches to a receptor.

Finally, exciting opportunities exist in atomic arrays and lattices with inverse population created by an appropriate (e.g., optical) pumping, which may lead to a laserlike locsiton stimulated emitter, to be discussed elsewhere.

XI. CONCLUSIONS

In conclusion, in this study of strong stratification of local field and dipole polarization in finite groups of atoms predicated by us earlier [1], we developed a detailed theory of the phenomenon in one-dimensional arrays of atom or resonant particles. In strong departure from Lorentz-Lorenz theory, the spatial period of those strata may become much shorter than the incident wavelength. By exploring nanoscale elementary excitations, locsitions, and resulting size-related resonances and large field enhancement in finite arrays of atoms, we showed that their spatial spectrum has both long waves, reminiscent of ferromagnetic domains, and super-short waves corresponding to the counteroscillating neigh-

boring polarizations, reminiscent of antiferromagnetic spins. The system also exhibits hybrid modes of excitation that have no counterpart in magnetic ordering, and are more representative of the effect. Our theory, which goes beyond Ising-type near-neighbor approximation and describes the excitation whereby each atom interacts with all the other atoms in the array, reveals the existence of infinite spectrum of exponential or “evanescent” eigenmodes in such arrays. We explored the phenomenon of magic numbers of atoms in an array, whereby resonant local-field suppression can be canceled for certain atoms in an array. We also demonstrated the existence of nonlinearly induced optical bistability and hysteresis in the system. We discussed a stratification effect similar to that in atomic arrays, which may exist in broad variety of self-interacting systems, from mechanical (pendulums) to electronic circuits, to radar arrays, and to the nuclear magnetic resonance. We pointed out a few potential applications of the atomic and similar arrays in such diverse field as low-loss nanoelements for optical computers, small-size Sagnac-effect-based gyroscopes, and biosensors.

ACKNOWLEDGMENTS

The authors appreciate helpful discussions with V. Atsarkin and R. W. Boyd. This work was supported by USAFOSR.

APPENDIX: MATHEMATICAL ASPECTS OF DISPERSION EQUATION (4.1)

In this appendix we consider mathematical properties of the Fourier series in dispersion relation (4.1), i.e., the function

$$\Sigma_\rho(q) \equiv \sum_{n=1}^{\infty} \frac{\cos(nq)}{n^\rho}, \quad (\text{A1})$$

which is a generalized form of Eq. (4.1) [in Eq. (4.1), $\rho=3$ due to the chosen geometry of the problem—1D array of point dipoles], but we will restrict ourselves to natural numbers ρ . Note, for example, that in the case of infinite “dipole strings,” parallel to each other and equidistantly arranged in a 2D plane, $\rho=2$, whereas for “dipole planes” parallel to each other and equidistantly arranged in the 3D space, $\rho=1$.

Our main purpose here is to find a closed finite analytical form of the function $\Sigma_\rho(q)$ that originated Fourier series (A1), and when it is impossible in terms of more or less regular analytical functions, at least find a closed finite derivative $d^m \Sigma_\rho(q)/dq^m$ with minimum derivative order m , which will help us to analyze in great detail the behavior of the function $\Sigma_\rho(q)$ in its physically interesting points, e.g., at $q=0, \pi$, the ratio between its minimum and maximum values, $\Sigma_\rho(\pi)/\Sigma_\rho(0)$, etc. Those derivatives are actually the main tool in our search. Indeed, differentiating $\Sigma_\rho(q)$ in Eq. (A1) $\rho-1$ times, one obtains

$$\frac{d^{\rho-1} \Sigma_\rho(q)}{dq^{\rho-1}} = (-1)^{\rho/2} \sum_{n=1}^{\infty} \frac{\sin(nq)}{n} \quad \text{if } \rho = 2, 4, 6, \dots \quad (\text{A2})$$

and

$$\begin{aligned} \frac{d^{\rho-1}\Sigma_\rho(q)}{dq^{\rho-1}} &= (-1)^{(\rho-1)/2} \sum_{n=1}^{\infty} \frac{\cos(nq)}{n} \\ &= (-1)^{(\rho-1)/2} \Sigma_1(k) \quad \text{if } \rho = 1, 3, 5, \dots \end{aligned} \quad (\text{A3})$$

Recalling that $\sin \xi = (e^{i\xi} - \text{c.c.})/2i$ and $\cos \xi = (e^{i\xi} + \text{c.c.})/2$, we recognize the sums $\sum_{n=1}^{\infty} e^{\pm inq}/n$ in Eqs. (A2) and (A3) as Taylor expansions of $-\ln(1 - e^{\pm iq})$.

In the case of even numbers ρ , sum (A2) in the interval $0, 2\pi$ (which is of the most interest) yields

$$\sum_{n=1}^{\infty} \frac{\sin(nq)}{n} = \begin{cases} \frac{\pi \operatorname{sgn}(q) - q}{2} & \text{if } |q| \in (0, 2\pi) \\ 0 & \text{if } |q| = 0, 2\pi. \end{cases} \quad (\text{A4})$$

It is discontinuous at $q=0, \pm 2\pi$. Even numbers ρ are thus a ‘‘lucky’’ case; result (A4) is easily integrated to restore function $\Sigma_\rho(q)$. In a physically interesting case, $\rho=2$, by integrating Eq. (A4) once we have

$$\Sigma_2(q) \equiv \sum_{n=1}^{\infty} \frac{\cos(nq)}{n^2} = \frac{3(\pi - |q|)^2 - \pi^2}{12} \quad \text{if } q \in [-2\pi, 2\pi], \quad (\text{A5})$$

which is a continuous (but not smooth) function with $\Sigma_2(0) = \pi^2/6$ and $\Sigma_2(\pi) = -\pi^2/12$, so that $(\Sigma_2)_{\min}/(\Sigma_2)_{\max} = -1/2$.

As to the closed integrability, one is not as lucky with odd numbers ρ ; the summation of Eq. (A3) yields

$$\Sigma_1(q) \equiv \sum_{n=1}^{\infty} \frac{\cos(nq)}{n} = -\ln[2|\sin(q/2)|], \quad (\text{A6})$$

i.e.,

$$\Sigma_1(q) \rightarrow \infty \quad \text{at } q = 2m\pi,$$

which cannot be integrated in simple known analytical functions, but it gives a good analytical tool for analysis of the behavior of $\Sigma_\rho(q)$. In the case of most interest to us, $\rho=3$, we have that near the maximum of Σ_3 at small wave numbers

$$\Sigma_3(q) \approx S + \frac{q^2}{2} \left(\ln|q| - \frac{3}{2} \right) \quad \text{at } |q| \ll 1, \quad (\text{A7})$$

where $S = \sum_{j=1}^{\infty} j^{-3} \approx 1.202057$, whereas near the minimum of Σ_3 , i.e., near $q = \pi$, we have

$$\Sigma_3(q) \approx -\frac{3S}{4} + \frac{(q - \pi)^2}{2} \ln 2 \quad \text{if } |q - \pi| \ll 1. \quad (\text{A8})$$

Notice that here $(\Sigma_3)_{\min}/(\Sigma_3)_{\max} = -3/4$, and $d^2\Sigma_3/dq^2 = 0$ at $q = 2m\pi \pm \pi/3$.

For the magic numbers in the case of full interaction of individual atoms with all the other atoms in the array, it is important to know zeros of the function $\Sigma_3(q)$. As it has been mentioned before [see Eq. (7.2) and related text], it turns out that the value of the ratio q'/π for the first positive root of the equation $\Sigma_3(q) = 0$ is very close to a small rational number:

$$\frac{q'}{\pi} = (1 + \Delta') \frac{6}{13}, \quad \text{with } \Delta' \approx 2.6 \times 10^{-4}. \quad (\text{A9})$$

For all practical purposes, a good approximation for $\Sigma_3(q)$ is provided by

$$\Sigma_3^{(\text{fit})}(q) = S \left\{ \cos q + \frac{\ln[(S + \Delta S)|\sin(q/2)|] \sin^2(q/2)}{\ln(S + \Delta S) \cdot 4} \right\}, \quad (\text{A10})$$

where $\Delta S = 0.01472$. It coincides with the results provided by numerical summation of Eq. (A1) with $\rho=3$ with the precision better than 0.6% of S , and their zeros coincide with each other and with Eq. (A9) with precision better than 10^{-6} .

Let us also prove the relation for $(\Sigma_\rho)_{\min}/(\Sigma_\rho)_{\max}$ used in Eq. (4.4). Indeed,

$$\begin{aligned} \frac{D(\pi, \rho)}{D(0, \rho)} &= \frac{(\Sigma_\rho)_{\min}}{(\Sigma_\rho)_{\max}} \\ &= \frac{\sum_{n=1}^{\infty} (-1)^n n^{-\rho}}{\sum_{n=1}^{\infty} n^{-\rho}} \\ &= \frac{-\sum_{n=1}^{\infty} n^{-\rho} + 2 \sum_{m=1}^{\infty} (2m)^{-\rho}}{\sum_{n=1}^{\infty} n^{-\rho}} \\ &= \frac{-\sum_{n=1}^{\infty} n^{-\rho} + 2^{-\rho+1} \sum_{n=1}^{\infty} n^{-\rho}}{\sum_{n=1}^{\infty} n^{-\rho}} \\ &= -1 + \frac{1}{2^{\rho-1}}. \end{aligned} \quad (\text{A11})$$

Note that Eq. (A11) is valid for any number $\rho > 1$.

- [1] A. E. Kaplan and S. N. Volkov, Phys. Rev. Lett. **101**, 133902 (2008).
 [2] M. Born and E. Wolf, *Principles of Optics* (Cambridge University Press, Cambridge, England, 1997), Secs. 2.3 and 2.4; J. Van Kranendonk and J. E. Sipe, in *Progress in Optics*, edited

- by E. Wolf (North-Holland, Amsterdam, 1977), Vol. 15, p. 245.
 [3] A. Aharoni, *Introduction to the Theory of Ferromagnetism* (Oxford University Press, Oxford, 2001).
 [4] L. D. Landau and E. M. Lifshitz, *The Classical Theory of Fields* (Butterworth, New York, 1980).

- [5] A. Yariv, *Quantum Electronics* (Wiley, New York, 1989); V. S. Butylkin, A. E. Kaplan, Yu. G. Khronopulo, and E. I. Yakubovich, *Resonant Nonlinear Interactions of Light with Matter* (Springer-Verlag, New York, 1989); V. S. Butylkin, A. E. Kaplan, and Yu. G. Khronopulo, *Sov. Phys. JETP* **32**, 501 (1971); C. M. Bowden and J. P. Dowling, *Phys. Rev. A* **47**, 1247 (1993).
- [6] J. J. Maki, M. S. Malcuit, J. E. Sipe, and R. W. Boyd, *Phys. Rev. Lett.* **67**, 972 (1991).
- [7] In general, the total homogeneous linewidth $\Gamma=2/T$ is comprised of two contributions [5]: one is the so-called natural radiation linewidth Γ_a , which is due to spontaneous radiation at the resonant frequency of the respective quantum transition of a single atom in vacuum, and the other one, Γ_{nr} , is due to all other processes, mostly phase-broadening, nonradiative transitions, and radiative ones to nonresonant quantum levels. It is worth noting that when the atoms are very close to each other, $l_a \ll \lambda$, due to atomic interactions the radiation linewidth Γ_a of each atom can be broadened up if the neighboring dipoles move in phase (as in long-wave locsitons), or narrowed down if those dipoles move in counterphase (as in short-wave locsitons). In general case this effect should be taken into consideration too. However, we assume here that, as is usual for atoms in a dense-material environment (e.g., when they are positioned at the surface of some material or embedded in it), $\Gamma_{nr} \sim \Gamma \gg \Gamma_a$, and we ignore here the natural linewidth Γ_a and its broadening.
- [8] D. G. Steel and S. C. Rand, *Phys. Rev. Lett.* **55**, 2285 (1985).
- [9] C. Kittel, *Introduction to Solid State Physics* (Wiley, New York, 1996).
- [10] E. Yablonovitch, *Phys. Rev. Lett.* **58**, 2059 (1987).
- [11] V. B. Sandomirskii, *Sov. Phys. JETP* **25**, 101 (1967); M. C. Tringides, M. Jałochowski, and E. Bauer, *Phys. Today* **60**(4), 50 (2007).
- [12] V. Chernyak, S. N. Volkov, and S. Mukamel, *Phys. Rev. Lett.* **86**, 995 (2001).
- [13] J. J. Stoker, *Nonlinear Vibrations in Mechanical and Electrical Systems* (Interscience, New York, 1950).
- [14] A. E. Kaplan, *Radio Eng. Electron. Phys.* **8**, 1340 (1963); A. E. Kaplan, Yu. A. Kravtsov, and V. A. Rylov, *Parametric Oscillators and Frequency Dividers* (Soviet Radio, Moscow, 1966), in Russian.
- [15] H. M. Gibbs, S. L. McCall, and T. N. C. Venkatesan, *Phys. Rev. Lett.* **36**, 1135 (1976); H. M. Gibbs, *Optical Bistability* (Academic, New York, 1985).
- [16] A. E. Kaplan, *Phys. Rev. Lett.* **48**, 138 (1982); **56**, 456 (1986).
- [17] O. N. Gadomskii and Yu. Yu. Voronov, *J. Appl. Spectrosc.* **67**, 517 (2000); O. N. Gadomskii and Yu. Abramov, *Opt. Spectrosc.* **93**, 879 (2002).
- [18] C. M. Bowden and C. C. Sung, *Phys. Rev. A* **19**, 2392 (1979).
- [19] M. P. Hehlen, H. U. Güdel, Q. Shu, J. Rai, S. Rai, and S. C. Rand, *Phys. Rev. Lett.* **73**, 1103 (1994).
- [20] S. I. Doronin, E. B. Fel'dman, and S. Lacelle, *Chem. Phys. Lett.* **353**, 226 (2002).
- [21] J. R. Long, in *Chemistry of Nanostructured Materials*, edited by P. Yang (World Scientific, Hong Kong, 2003).
- [22] J. R. Heath and M. A. Ratner, *Phys. Today* **56**(5), 43 (2003).
- [23] A. K. Sarychev and V. M. Shalaev, *Electrodynamics of Metamaterials* (World Scientific, Hong Kong, 2008); W. A. Murray and W. L. Barnes, *Adv. Mater. (Weinheim, Ger.)* **19**, 3771 (2007); *Surface Plasmon Nanophotonics*, edited by M. L. Brongersma and P. G. Kik (Springer, New York, 2007); Y. Fainman, K. Tetz, R. Rokitski, and L. Pang, *Opt. Photonics News* **17**(7), 24 (2006).
- [24] I. Žutić, J. Fabian, and S. Das Sarma, *Rev. Mod. Phys.* **76**, 323 (2004).